International Institute of Welding
*A world of joining experience*

Delegation of Sweden

IIW Document XIII-2175-07

# Fatigue Assessment and LEFM Analysis of Cruciform Joints Fabricated with Different Welding Processes

**Z. Barsoum[1] and B. Jonsson[2]**
[1]Royal Institute of Technology
Dep. of Aeronautical and Vehicle Engineering
100 44 Stockholm, Sweden
zuheir@kth.se

[2] Volvo CE HL Divisions
360 42 Braås, Sweden
bertil.bj.jonsson@volvo.com

corresponding author: zuheir@kth.se

**Keywords:** Fatigue testing, stress concentration, weld defects, residual stress, welding processes, and LEFM.

**Abstract**

In this study fatigue testing and defect assessment were carried out on specimens welded with robotic and manual welding using flux cored (FCAW) and metal cored (MCAW) filler materials in order to study the effect of the welding method on the fatigue strength and weld quality. Thirteen different batches were investigated of which two was shot peened before fatigue testing. The local weld geometry was measured for all the specimens before testing. The specimens welded with flux cored weld wire showed the best fatigue strength, small defects and low residual stresses. Large scatter in the fatigue data is observed, especially when manual welding is employed. The few largest defects were removed by the shot peening process, although small defects survived. This led to a smaller scatter in fatigue live for the shot peened specimens. Linear elastic fracture mechanics, LEFM, was employed for analysis of the fatigue test results. The fatigue life predictions using a 2D LEFM FE-model for simulating a continuous cold lap defect along the weld toe showed a qualitative agreement with the fatigue test results. The 2D analysis showed that a continuous cold lap defect should be no more than 0.5 mm deep in order to comply with the requirement of fatigue lives for normal weld quality according to the IIW design rules. For larger defects (>0.8 mm) an increased toe radius will have a small effect on the fatigue strength. A 3D LEFM analysis of crack growth from a spatter -induced cold lap defect was also carried out. This showed similar trends in crack growth compared to the 2D analysis of a continuous cold lap, although the spatter-induced cold lap defect (semi-elliptical) had a longer fatigue life (x2.7), and hence is less dangerous from a fatigue point of view.

## Introduction

To increase the utilization of high strength steel in fatigue loaded welded structures it is necessary to improve design and to increase weld quality. The variation in weld quality will cause scatter in fatigue life and a better understanding of the relation between fatigue life and weld quality would enable manufacturers to gain advantage in terms of increased design

stresses for producing higher quality welds. Extensive research has been carried out within the Nordic research projects with the emphasis on the fatigue strength of welded joints in relation to weld quality, i.e. weld defects and local weld geometry [1-7].
In this paper welding processes are studied in relation to the fatigue strength and weld quality achieved using different welding methods. Six weld batches were produced with manual MCAW, four with robot MCAW in factory A and, three with manual FCAW in factory B. The specimens were welded with different weld fillers. Fatigue testing was carried out in order to obtain the fatigue strength.
Residual stress measurements were made at the weld toe, the location of fatigue failure, on specimens in some of the batches. The local toe geometry (toe radius and toe angle) was measured for every specimen and the stress concentration factor was calculated. Furthermore, two of the batches were shot peened in order to introduce compressive residual stresses, and then fatigue tested. The local weld geometries before and after shot peening were analyzed and compared. The fatigue test results were assessed using the nominal stress and the notch stress at the weld toe, as recommended by the IIW [8]. Finally, linear elastic fracture mechanics (LEFM) was employed to carry out fatigue assessments of the weld defects.

## Test specimens

The fatigue tests were performed on steel non-load carrying welded cruciform joint specimens. These were manufactured from plates which were shot blasted before welding in order to clean the surface to avoid the development of cold laps and other types of lack of fusion. The panels were cut up in 10 specimens, each 12 mm thick and 12 mm wide, see figure 1. These batches were produced in two different plants:

- Six manual welded batches (MCAW) - factory A
- Four robotic welded batches (MCAW) - factory A
- Three manual welded batches (FCAW) - factory B

The panels were welded with different brands of weld filler materials for MCAW and FCAW in the two different factories A and B. A detailed study of the fatigue strength of the different weld filler materials is presented in Barsoum [1].
Table 1 shows the material properties for the steel grades used in the two factories. The welding in factory A was performed in the best position (PA) while that in factory B was performed in the flat horizontal position.

***Table 1**. Mechanical properties of the materials.*

| **Factory (Base steel material)** | $\sigma_Y$ **-** $R_P0.2$ **(MPa)** | $\sigma_B$ **-** $R_M$ **(MPa)** | ***HV* 10** | ***A10%*** | $R_P0.2/R_M$ |
|---|---|---|---|---|---|
| **A** | 390 | 540 | 164 | 22.4 | 0.72 |
| **B** | 490 | 600 | 175 | 21.2 | 0.82 |

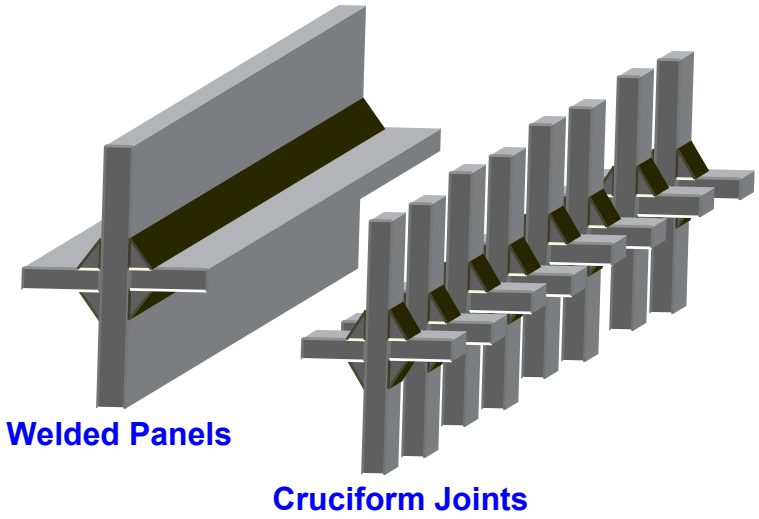


***Figure 1.*** *Test specimens from welded panels.*

## Local weld geometry

For the measurement of the local weld geometries, silicon imprint samples of every weld of the test specimens were made. The silicon samples were cut into several thin slices, copied and enlarged on a photocopier. In some cases, measurement of the weld toe radius was difficult due to the sharp transition between the weld material and the main plate. In these cases, a toe radius of 0.1 mm was assumed in order to calculate the stress concentration factor. Figure 2a-c show the results from the local weld geometry measurements, toe radius and toe angle, for robotic MCAW, manual MCAW and manual FCAW, respectively. The local weld geometry measurements for the manual FCAW test specimens show smaller toe radii and less scatter compared with robotic and manual MCAW specimens. The manual FCAW of specimens were cleaned to remove loose surface slag before the measurements. Two batches from factory A, one manual and one robotic welded with MCAW were shot peened and the local weld geometry was measured before and after the shot peening. Figure 2d shows the relation between radius and toe angle before and after shot peening. After shot peening the majority of the points are below the curve $K_t = 2.5$, defined as the SCF for an even transition. All combinations of toe radius and toe angle that results in a calculated $K_t$ below 2.5 are defined as a weld having an even transition [3]. The SCF calculations are carried out using a parametric linear elastic FE model developed in ANSYS for cruciform welded joints. The shot peening removed slag and larger spatter along the weld toe, including the thin slag layer along weld toe line. This revealed a smaller toe radius and toe angle than that measured before the slag was removed. As a consequence, the true stress concentration factor is higher in these cases. Table 2 show the changes in the geometry before and after shot peening for the two batches. This is in agreement with earlier research within the Nordic project. In Lopez et al [9], extensive fatigue testing, defect characterisation and local weld geometry measurement was carried out on non-load carrying cruciform joints welded with e.g. FCAW. The local weld geometry, toe radius and toe angle were documented by plastic replica. Calibration showed that the measurement method used gave reasonable accuracy only if the weld toe area was cleaned enough.

From the results presented in table 2 and figure 2, the accuracy of the present local weld geometry measurement technique could be questionable, since the thin slag covers the true toe radius when no cleaning is employed; this makes measurement complicated.

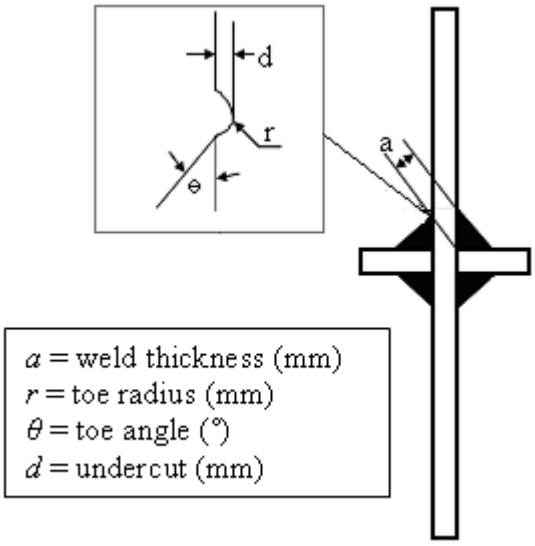


a)

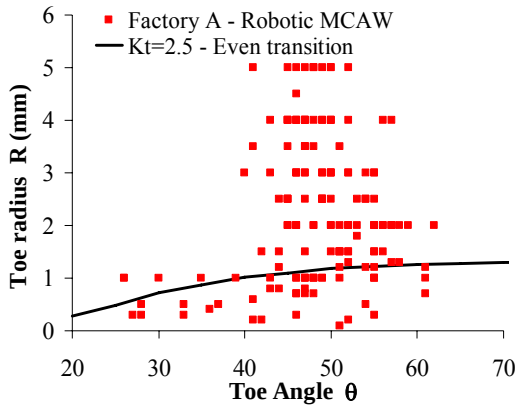


b)

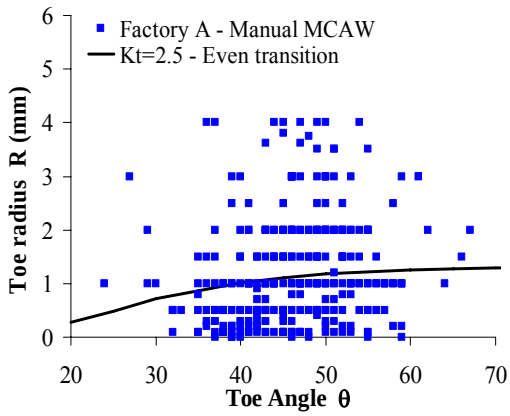


c)

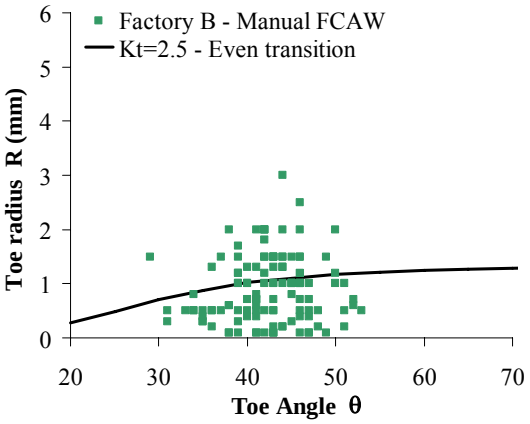


d)

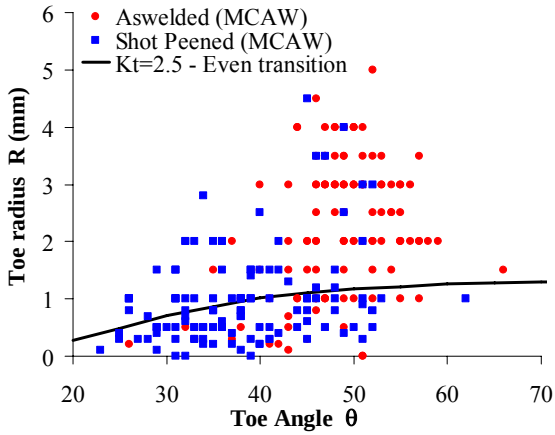


e)

***Figure 2.*** *Local weld geometry: a) Cruciform joint and local weld geometry measurements ; b) Factory A (Robotic MCAW); c) Factory A (Manual MCAW); d) Factory B (Manual FCAW); e) before and after shot peening.*

***Table 2.*** *Local weld geometry before and after shot peening.*

| *m* = mean value<br>*S* = standards deviation | | ***R* (mm)** | | ***Theta* (°)** | | **$K_t$** | |
|---|---|---|---|---|---|---|---|
| | | *m* | *S* | *m* | *S* | *m* | *S* |
| **Manual MCAW** | As-welded | 1 | 0.5 | 50.6 | 10.6 | 2.7 | 0.4 |
| | Shot Peened | 0.6 | 0.3 | 44 | 15.9 | 2.9 | 0.3 |
| | | | | | | | |
| **Robotic MCAW** | As-welded | 2.7 | 1.1 | 49.5 | 5.1 | 2.1 | 0.6 |
| | Shot Peened | 0.9 | 0.8 | 36.6 | 6.8 | 2.8 | 0.7 |

## Residual Stresses

Residual stresses measurements were carried out by X-ray diffraction on some specimens fabricated in both factories. Residual stress measurements were also carried out on a shot peened specimen. The measurements were made less than 1 mm from the weld toe on the main plate and the results are presented in table 3.
As will be seen, the residual stresses were sometimes tensile but mainly compressive in the as-welded specimens, but they were always compressive in the shot peened specimens. This is in agreement with the results by Barsoum *et al* [2] where compressive residual stresses were measured at the weld toes for as-welded non load-carrying cruciform joints of the same size and welded with FCAW.

***Table 3.*** *Residual stresses measured in specimens from factory A and B.*

| **Measurement Positions** | **Factory A (MCAW)** | | | **Factory B (FCAW)** | | |
|---|---|---|---|---|---|---|
| | Robotic | Manual | Manual (Shot peened) | Robotic | Manual | 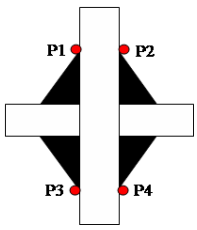 |
| **P1 [MPa]** | -102 | -74 | -213 | - | -74 | |
| **P2 [MPa]** | -102 | 12 | -277 | - | -35 | |
| **P3 [MPa]** | -117 | 48 | -154 | - | 119 | |
| **P4 [MPa]** | 62 | -43 | -243 | - | -115 | |

## Fatigue test results

The fatigue testing was carried out in a MTS machine (max: ±50 kN, 15 Hz) using constant amplitude, pulsating tension ($R$ = 0). The fatigue testing and defect detection and characterisation were carried out as in previous studies, Barsoum et al. [2]. The IIW [8] recommendation of the fatigue design strength of non-load carrying cruciform joints is 80 MPa, the fatigue strength at 2 million cycles for a 5% failure probability (*FAT*). The corresponding experimental fatigue strength at 2 million cycles was calculated according to the procedure outlined in IIW [8] by first fitting the mean S-N curve of the form $\log(N) = \log(C) - m*\log(S)$ and assuming a slope of $m = 3$, and then establishing the 5% probability of

failure line a number of standard deviations of log (*N*) below it, the number depending on the number of fatigue test results, see table 4.

Table 4 and figure 4 summarise the results of the fatigue tests and the resulting *S*-*N* curves for the batches from factory A (manual and robotic MCAW) and factory B (manual FCAW). The shot peened batches show higher slope, *m*, and fatigue strength above the IIW recommendation *FAT* 80 compared with the as welded batches.

Slightly higher fatigue strength was found in the robotic MCAW compared to the manual MCAW. Many weld defects e.g. spatter, slag and oxide were found in the robotic MCAW batch and this could be the reason for the large scatter observed in the fatigue test results for this batch together with the scatter observed in the local weld geometry measurement, see figure 3. Weld defects, cold laps, were also found in the shot peened batches - some weld defects survived the shot peening process.

Smaller scatter was observed in the fatigue test results for the manual FCAW batch from factory B. This was possibly due to the cleaning of the specimens after welding since small defects were found in some of the specimens only after the fatigue testing.

Tables 5-7 summarize the test result for the individual weld filler material used in the different welding processes. These are also published elsewhere by Barsoum [1]. The fatigue strengths for the individual manual MCAW weld filler are all below the fatigue strength recommendation *FAT* 80, except the shot peened specimens. Most of the fillers that gave fatigue strengths above *FAT* 80 were from the robotic MCAW and manual FCAW batches, some being significantly above *FAT* 80.

***Table 4.*** *Summarizing result for factory A (manual and robotic MCAW) and factory B (manual FCAW), respectively.*

| **Mean value / Standard deviation** | **MCAW** | | | | **FCAW** | **All Specimens** |
|---|---|---|---|---|---|---|
| | **Manual** | | **Robotic** | | **Manual** | |
| | ***As welded*** | ***Shot Peened*** | ***As welded*** | ***Shot Peened*** | ***As welded*** | ***As welded*** |
| **Failed/Run outs** | 40/1 | 5/1 | 23/4 | 8/2 | 28/1 | 110/7 |
| $K_t$ * | 3.4/1.2 | 2.9/0.3 | 2.5/0.5 | 3.3/0.5 | 3.2/1.0 | - |
| **Toe radius (mm)** | 0.95/0.9 | 0.6/0.3 | 1.4/0.8 | 0.9/0.8 | 0.73/0.5 | - |
| **Toe angle (˚)** | 49/7.5 | 44/15.9 | 49/9.8 | 36.6/6.8 | 43/4.9 | - |
| **Weld thickness (mm)** | 6/0.3 | 6/0.3 | 5.4/0.2 | 5.4/0.2 | 5.7/0.2 | - |
| **Cold laps (mm)** | 0.09-0.15 | 0.09/0.04 | 0.13-0.27 | 0.12/0.04 | 0.1-0.2 | - |
| ***m* – slope** | 2.8 | 3.6 | 2.8 | 4 | 3.2 | - |
| **Log *C* (*m* = 3)** | 12.28/0.209 | 12.53/0.071 | 12.4/0.256 | 12.53/0.108 | 12.4/0.178 | 12.39/0.237 |
| **Nr of standard dev.** | 2.09 | 3.58 | 2.26 | 2.91 | 2.19 | 1.9 |
| ***FAT* at $P_f$ 50% (*N* = 2e6, *m* = 3)** | **98** | **119** | **110** | **120** | **106** | **107** |
| ***FAT* at $P_f$ 5% (*N* = 2e6, *m* = 3)** | **71** | **98** | **70** | **94** | **80** | **76** |

*) Calculated $K_t$ based on actual measured weld toe angle and radius.

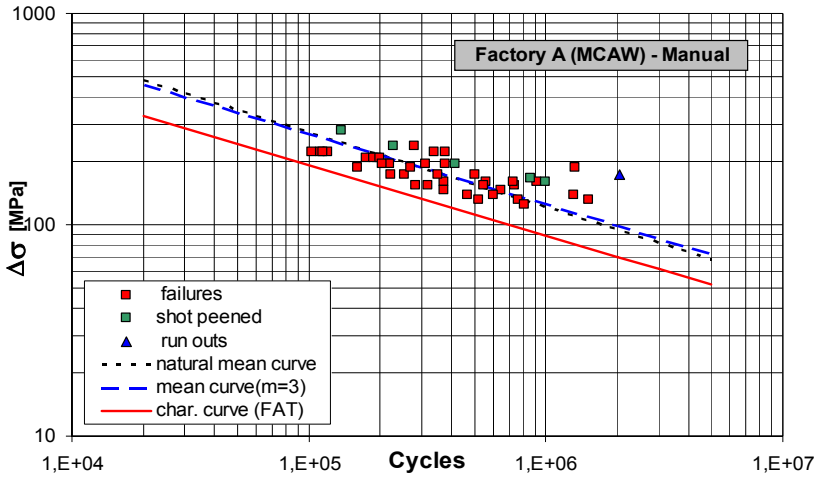


a)

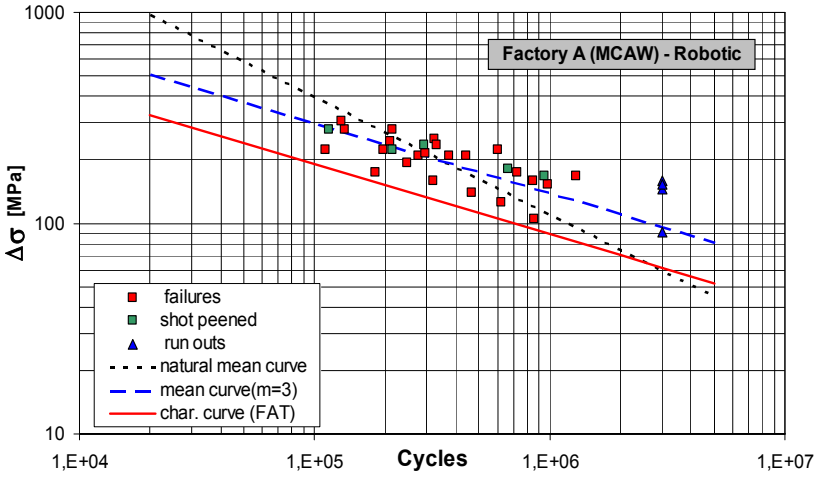


b)

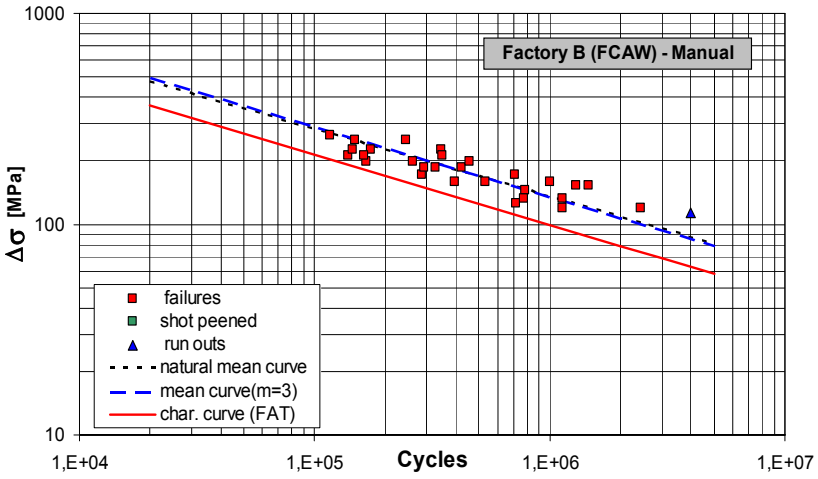


c)

***Figure 3.*** *Fatigue test result compiled in S-N-curves: Factory A; (MCAW) a) manual; b) robotic, Factory B (FCAW); c) manual. Δσ is the nominal stress range at stress ratio R = 0.*

***Table 5.*** *Summary of test result for individual weld filler materials in manual MCAW batch, Barsoum [1].*

| **Mean value / Standard deviation** | **FM-1** | **FM-2** | **FM-3 Shot peened** | **FM-4** | **FM-5** | **FM-6** |
|---|---|---|---|---|---|---|
| $K_t$ | 3.8/1.3 | 2.2/0.2 | 2.9/0.3 | 3.4/1.1 | 4.1/1.2 | 2.6/0.4 |
| **Cold lap (mm)** | 0.09/0.02 | 0.12/0.01 | 0.09/0.04 | 0.15/0.07 | 0.14/0.04 | 0.12/-- |
| ***m*-natural slope** | 4.5 | 6 | 3.6 | 2.9 | 3.2 | 3.3 |
| **Log *C* (*m* = 3)** | 12.25/0.183 | 12.68/0.25 | 12.53/0.071 | 12.24/0.13 | 12.20/0.166 | 12.23/0.164 |
| **Nr of standard dev.** | 2.8 | 3.27 | 3.58 | 2.8 | 2.8 | 2.91 |
| ***FAT* at $P_f$ 50% (*N* = 2e6, *m* = 3)** | 96 | 134 | 119 | 96 | 93 | 95 |
| ***FAT* at $P_f$ 5% (*N* = 2e6, *m* = 3)** | 65 | 71 | 98 | 71 | 65 | 66 |

***Table 6.*** *Summary of test result for individual weld filler materials in robotic MCAW batch, Barsoum [1].*

| **Mean value / Standard deviation** | **FM-7** | **FM-8** | **FM-9 Shot peened** | **FM-10** |
|---|---|---|---|---|
| $K_t$ | 2.7/0.2 | 2.2/0.3 | 3.3/0.5 | 2.6/0.6 |
| **Cold lap (mm)** | 0.16/0.05 | 0.27/0.12 | 0.12/0.04 | 0.13/0.01 |
| ***m*-natural slope** | 2.3 | 3.5 | 3.9 | 3.4 |
| **Log C (*m* = 3)** | 12.13/0.13 | 12.51/0.091 | 12.53/0.10 | 12.65/0.121 |
| **Nr of standard dev.** | 2.91 | 3.06 | 2.91 | 2.91 |
| ***FAT* at $P_f$ 50% (*N* = 2e6, *m* = 3)** | 87 | 117 | 120 | 130 |
| ***FAT* at $P_f$ 5% (*N* = 2e6, *m* = 3)** | 64 | 95 | 94 | 99 |

***Table 7.*** *Summary of test result for individual weld filler materials in manual FCAW batch, Barsoum [1].*

| **Mean value / Standard deviation** | **FM-11** | **FM-12** | **FM-13** |
|---|---|---|---|
| $K_t$ | 3.5/1 | 3.3/1.3 | 2.8/0.5 |
| **Cold lap (mm)** | 0.10/0.03 | 0.28/0.05 | 0.22/0.11 |
| ***m*-natural slope** | 3.7 | 3 | 3.4 |
| **Log *C* (*m* = 3)** | 12.30/0.15 | 12.27/0.084 | 12.58/0.08 |
| **Nr of standard dev.** | 2.7 | 2.8 | 2.8 |
| ***FAT* at $P_f$ 50% (*N* = 2e6, *m* = 3)** | 100 | 97 | 124 |
| ***FAT* at $P_f$ 5% (*N* = 2e6, *m* = 3)** | 73 | 81 | 104 |

## Fatigue assessment using effective notch stress method

The effective notch stress is the total stress at the root of a notch, e.g. at the weld toe radius, obtained assuming linear-elastic material. To take into account variations in the weld shape, the real weld contour is replaced by an effective and fictitious notch root radius of 1 mm. This fictitious notch radius has to be added to the actual notch radius, which is usually assumed to be zero in a conservative way (worst case assumption). Therefore it is recommended to assume generally $R$ = 1 mm for design purposes, see figure 4. The fatigue tests from factory A and B were assessed according to the effective notch stress method as outlined in the recommendations in [8]. The effective notch stress was calculated for each specimen assuming an effective weld toe radius (1 mm) and excluding the actual notch radius and the toe angle was set to $\varphi_{mean}$ = 49˚ which resulted in $K_t$ = 2.6. The shot peened specimens are excluded from the evaluation. The method does not consider any misalignment of the specimen, which for these specimens could introduce secondary bending stress. However, the misalignment was considered as small and was not taken into account. The resulting effective notch stress ranges are plotted versus the observed lives in figure 5. Table 8 summarise the assessment of the fatigue test results using the effective notch stress method. The characteristic curve ($P_{5\%}$ = 194 MPa) for all the specimens is below the characteristic curve, *FAT* 225 MPa, recommended by IIW. This is due to the worst case assumption (toe radius =1 mm) in connection with high scatter in the local weld geometry and observed lives with a standard deviation of 0.229 for Log (*C*).

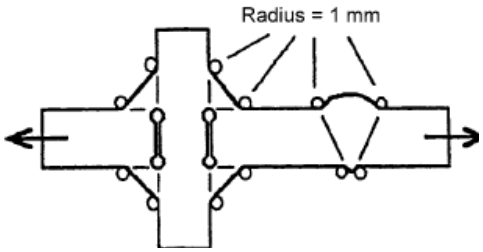


***Figure 4.*** *Fictitious rounding of weld toes and roots [8].*

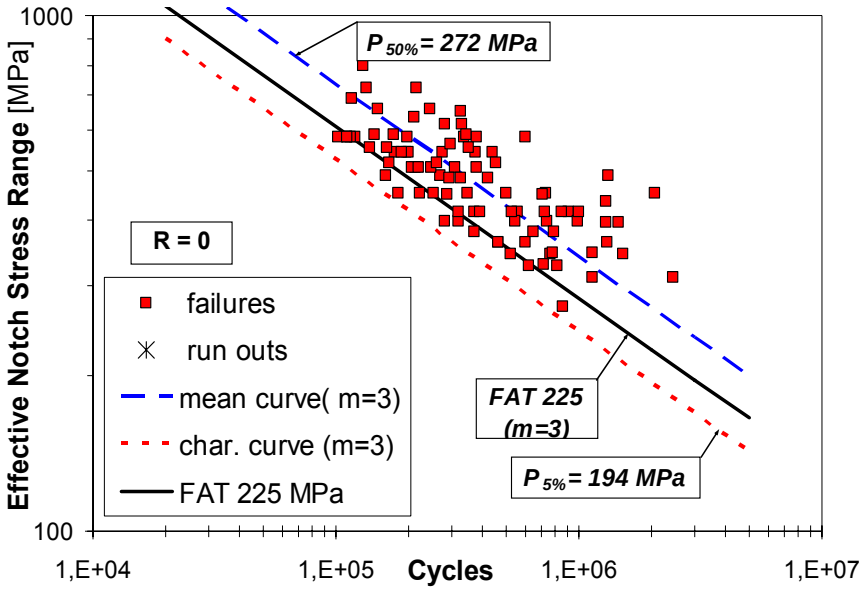


***Figure 5.*** *Evaluation of fatigue test results using the IIW [8] effective notch stress method.*

***Table 8.*** *Evaluation of fatigue test result of as welded specimens using effective notch stress method according to IIW [8].*

| Mean value / Standard deviation | MCAW | | FCAW | All Specimens |
|---|---|---|---|---|
| | Manual | Robotic | Manual | |
| | *Effective notch radius 1 mm* | | | |
| **Toe radius (mm)** | 0.95/0.9 | 1.4/0.8 | 0.73/0.5 | 1.15/0.8 |
| **Log *C* (*m* = 3)** | 13.54/0.252 | 13.67/0.236 | 13.60/0.183 | 13.60/0.229 |
| **Nr of standard dev.** | 2.08 | 2.26 | 2.19 | 1.92 |
| ***FAT* at $P_f$ 50% (*N* = 2e6, *m* = 3)** | **258** | **287** | **270** | **272** |
| ***FAT* at $P_f$ 5% (*N* = 2e6, *m* = 3)** | **173** | **191** | **199** | **194** |

## LEFM fatigue analysis

Weld defects, cold laps and undercuts of varying size and shape, are often present at the weld toe in welded joints. As illustrated previously in this paper, table 4, weld defects were found in the majority of the batches analyzed and this, together with the variation in local weld geometry, will increase the scatter in the fatigue data. The most frequent type of defect in a single run weld for many welding methods, including MCAW and FCAW, is a cold lap; a defect mainly parallel to the plane of the parent metal plate surface.

In Signes et al [10] fatigue cracks at the toes of welded joints were shown to initiate from small defects in form of cold laps and sharp slag. These were in the range 0.15-0.4 mm in depth. In Lopez et al [11-12] a comprehensive investigation of defects in fillet welds was carried out for MAG welded cruciform joints. The majority (80 %) of the observed defects were defined as cold laps 0.05-0.27 mm, but a few large as 1.4 mm.

A weld defect assessment was carried out in order to study the range of the defect sizes detected in the specimens from the different welding processes and their effect on the fatigue life. For this purpose linear elastic fracture mechanics (LEFM) was employed. The total fatigue life of welds involves both a crack initiation and crack propagation stage. For welded joints an initial crack is assumed to exist due to the presence of weld defects and the major part of the fatigue life is consumed by propagation. This is a conservative way of predicting fatigue life in some cases, especially if a defect is assumed to take the form of a straight-fronted 'line' crack (depth/surface length $a/2c = 0$).

The software used for calculating the fatigue life in the critical welds were the LEFM code Franc2d [13] and the LEFM weight function code Afgrow [14].

The Paris crack growth law for mode I cracks, equation 1, was used for the analysis, with the crack growth parameters for 50% failure probability proposed by IIW [8], $C_{mean} = 4.75*10^{-12}$ MPa√m, $C_{char} = 9.5*10^{-12}$ MPa√m and $m = 3$,. Threshold effects were considered by assuming a $\Delta K_{th} = 2$ MPa√m. $K_c$ is the critical stress intensity factor (unstable fracture).

$$\frac{da}{dN} = C \cdot \frac{(\Delta K)^m}{(1 - R_{eff})}, \qquad (\Delta K \geq \Delta K_{th},\ K_{\max} \leq K_c,\ R = 0) \tag{1}$$

The residual stresses were incorporated in the LEFM fatigue life analysis by assuming the average measured values; -100 MPa for the as welded and -200 MPa for the shot peened specimens, respectively. The magnitude of the residual stress is assumed to be constant 1 mm trough the thickness, thereafter it is assumed to be relaxed to zero. In this application $K_{residual}$ was added to the stress intensity factor caused by the minimum and maximum applied loads, equation (2). This will not change the applied $\Delta K$, but will change the stress ratio, which will result in a change in the crack growth rate.

$$R_{eff} = \frac{\left(K_{\min} + K_{residual}\right)}{\left(K_{\max} + K_{residual}\right)} \tag{2}$$

The theoretical fatigue strength (*FAT*) at $2*10^6$ cycles for 95% survival probability was determined by adjusting the mean *S*-*N*-curve [15], equation (3).

$$\Delta\sigma^m N = \frac{I}{C\sqrt{t}} \qquad (t = \text{thickness},\ I = \text{crack propagation integral}) \tag{3}$$

On the basis of equation 3 the corresponding characteristic (*FAT*) fatigue strength is given by;

$$FAT = \sqrt[3]{\frac{C_{mean}}{C_{char}}}\Delta\sigma_{mean} = 0.7937\Delta\sigma_{mean} \tag{4}$$

***Modelling of weld defects***

Figure 6 shows a simulation of crack propagation from a 0.3 mm cold lap and a 0.03 mm line crack to the half thickness in a non-load carrying cruciform welded joint. Due to the horizontal shape of the cold lap mixed mode crack growth will occur and result in a higher $\Delta K_{II}$ than the line crack during the first crack growth increment. $\Delta K_{II}$ decreases when the crack has propagated to approximately 0.3 mm and the cold lap continues to propagate as a straight-fronted edge crack, and after 1 mm of crack growth 70% of the life is consumed. Figure 7 shows the stress intensity factor (SIF, Mode I) for different cold lap and line crack sizes at different growth increments. The SIF reaches a fairly constant level for all cold lap sizes after ~0.3 mm of growth, figure 7a, and the cold lap will grow in the shape of a line crack in the subsequent growth increments. Calculations in [16] showed that reasonable fatigue life estimates were obtained if it was assumed that a cold lap was equivalent to a line crack 10% of the actual cold lap size. The crack growth simulations from a cold lap in figure 6-7 show good correlation with the cold lap defects detected in the microscopic investigation of the fracture surfaces; multiple cold laps links up and forms a straight-fronted surface crack early in the propagation stage, as can be seen in figure 8.

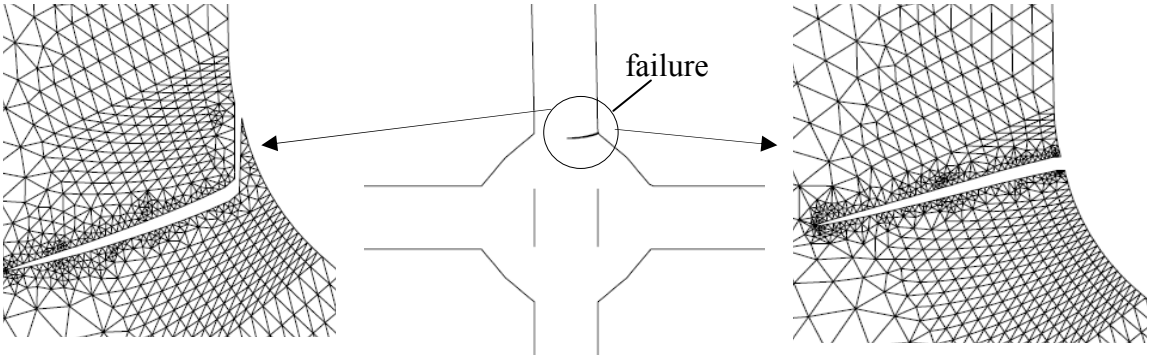


***Figure 6.*** *Simulation of fatigue crack propagation from: a) a cold lap (0.3 mm) and b) a straight-fronted line crack (0.03 mm).*

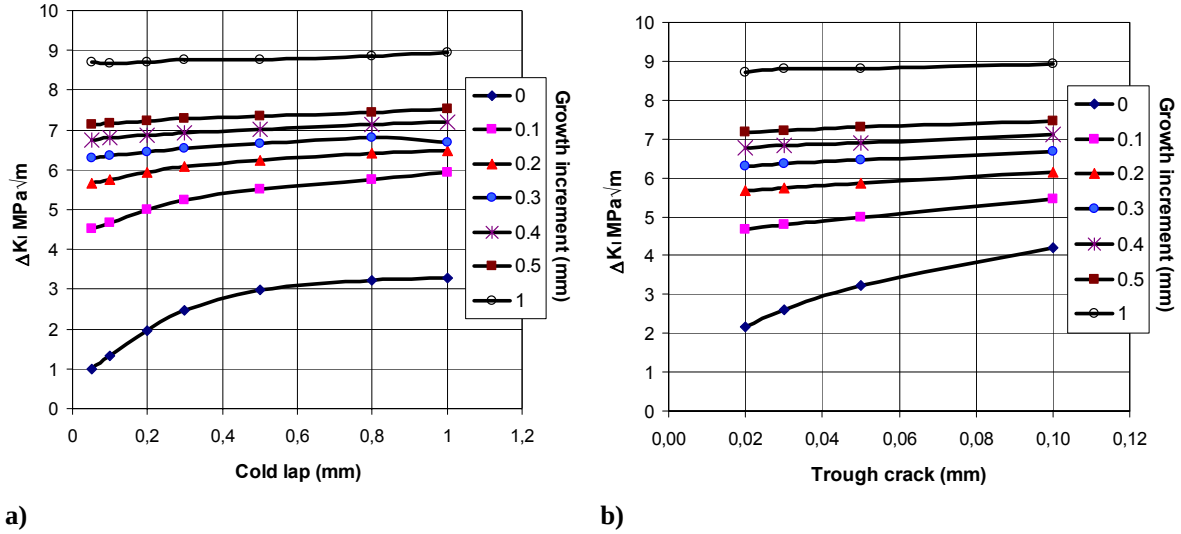


***Figure 7.*** *Stress intensity factor as function of defect size and growth increment: a) cold lap; b) straight-fronted line crack.*

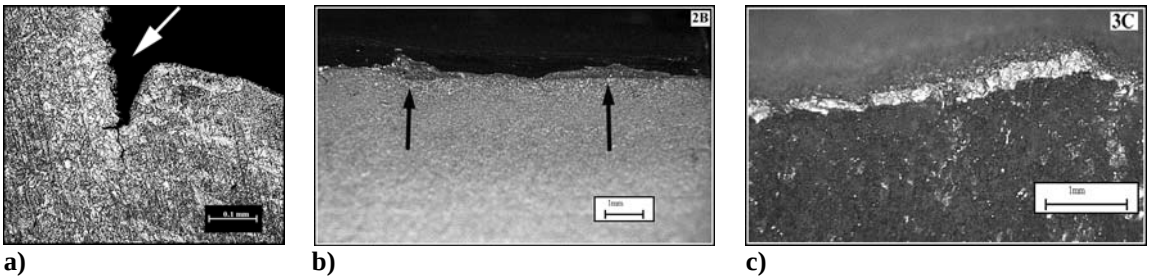


***Figure 8.*** *Microscopic investigation of fracture surface and weld defects: a) 0.3 mm initial cold lap; b) multiple cold laps along spatter band; c) a 0.1 mm straight-fronted surface crack.*

Figure 9 shows the stress intensity factors and the fatigue lives for a nominal applied stress range of $\Delta\sigma_{nom}$ = 100 MPa and $K_t$ = 2.5 for the different crack shapes analyzed: a straight-fronted surface crack ('line' crack), a semi elliptical surface flaw and a cold lap defect. The

$\Delta K_I$ values obtained by the weight function are non-conservative since the weight function solution does not consider any redistribution of the applied stress when the crack propagates. When integrating the Paris law for the fatigue life, the weight function solution in Afgrow [14] uses a piecewise increasing *da/dN* curve. Otherwise, integrating the $\Delta K$ *(a)* for the weight function line crack using constant *da/dN* will give very short fatigue lives.
The semi-elliptical surface flaw shows a 40% higher crack growth rate at the surface compared with crack growth in the depth direction and will form a straight-fronted surface crack. The line crack and the cold lap defect show similar trends although the cold lap will have a higher $\Delta K_{II}$ than the vertical crack during the first phase of the crack growth. Table 9 summarizes the crack sizes together with initial $\Delta K_I$ for the different defects analysed.

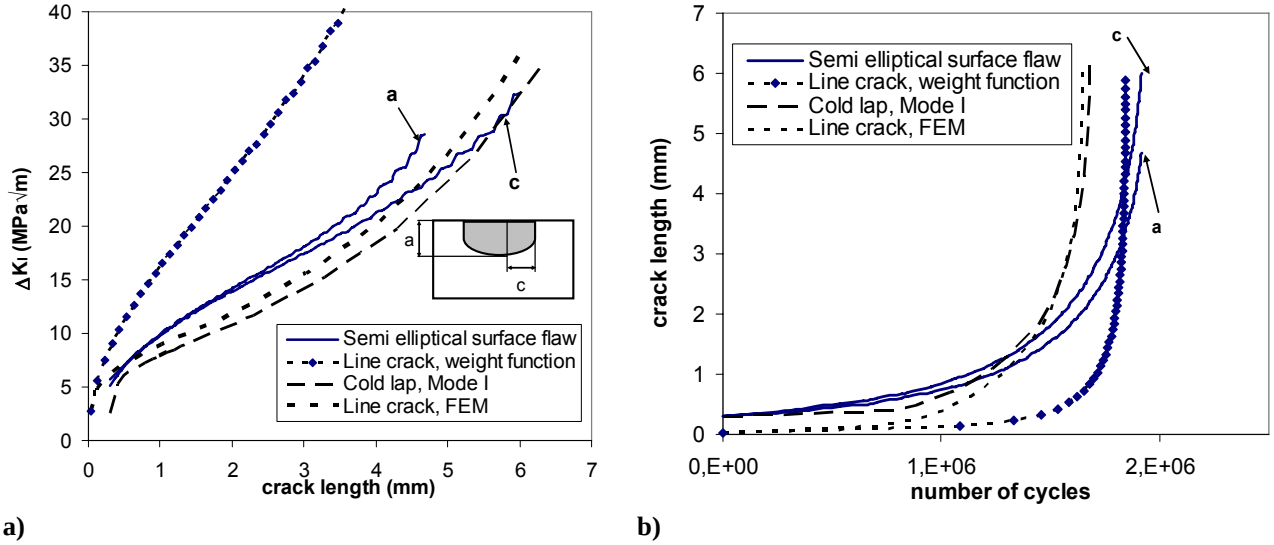


***Figure 9.*** *Behaviour of different crack shapes: a) stress intensity factors; b) fatigue life.*

***Table 9.*** *Comparison between different crack sizes analyzed in figure 9.*

| $\Delta\sigma_{nominal}$ = 100 MPa  $K_t$ = 2.5 | | |
|---|---|---|
| ***Weight function*** | $c_i/a_i$ (mm) | $K_{I,i}$ (MPa√m) |
| Semi elliptical crack | 0.3/0.3 | 5.7/5.1 |
| Line crack | 0/0.03 | 2.7 |
| | | |
| ***FEM*** | $a_i$ (mm) | $K_{I,i}$ (MPa√m) |
| Cold lap (Mode I) | 0.3 | 2.5 |
| Line crack | 0.03 | 2.6 |

### *Influence of defects on the fatigue strength (FAT)*

The characteristic fatigue strength (5% failure probability) for non load carrying cruciform joints was calculated for different sizes of cold lap defects and semi elliptical surface flaws at different toe radii and stress concentrations, see figure 10. The dashed lines are fatigue strengths calculated assuming that the crack growth law continues for $\Delta K_I$ values below $\Delta K_{th}$ = 2 MPa√m. The fatigue strengths calculated for the cold lap defects shows no increase for

cold laps larger than 0.5 mm ($0.1 \leq R \leq 2$ mm) and for larger defects (>0.8 mm) the small $K_t$ (increased $R$) will have a small effect on the fatigue strength. This is due to the local nature of the stress concentration. For smaller cold lap defects (<0.8 mm) the effect of an increased toe radius on the fatigue strength is more pronounced. The IIW fatigue strength recommendations for non-load carrying cruciform joints *FAT*80 marked in figure 10 shows the defect size acceptance limit over the stress concentration range $3.1 \leq K_t \leq 2.0$; for cold lap defects $0.1 \leq a \leq 0.4$ mm and for semi elliptical surface flaws $0.1 \leq (a, c) \leq 0.6$ mm. The weld defects found in the investigated specimens are within these intervals. In order to ensure the production of a weld with fatigue strength above the standard recommendation *FAT*80, the weld toe radius should be larger than 1 mm (even transition) and the cold lap defect size not larger than 0.5 mm, see figure 10.

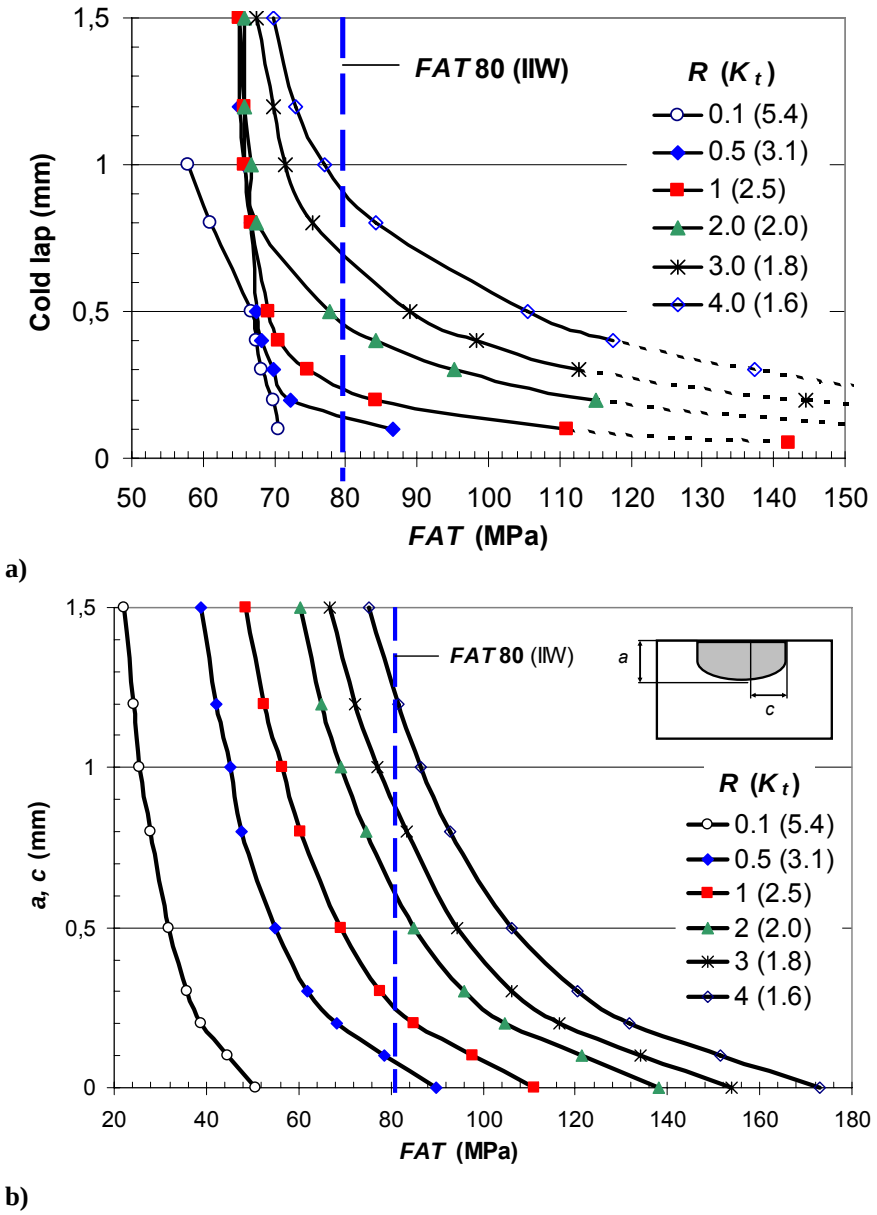


***Figure 10.*** *Fatigue strength (FAT) for different toe radius (R), stress concentration ($K_t$) and crack size: a) cold lap defect; b) semi elliptical surface flaw. The dashed lines indicate FAT values at $\Delta K_I < \Delta K_{th}$ (2 MPa$\sqrt{m}$).*

## *Fatigue life prediction*

The predicted and experimental fatigue lives for the as welded and shot peened conditions at selected nominal stress ranges for all the non-load carrying welded joints are summarized in figure 11. The prediction shows good correlation with the experiments, although the fatigue test results are scattered. The local weld geometry, residual stresses and crack growth data used were the average values. A 0.05 mm initial line crack is assumed as a starting crack at the weld toe. At longer fatigue lives (>1 million cycles) the predictions are non-conservative due to the assumption of constant residual stress distribution, i.e. no residual stress relaxation/redistribution. Also a crack initiation period and threshold effect could have an influence on the fatigue life prediction at cycles larger than one million cycles. Figure 12 illustrates the scatter associated with the experimental and predicted fatigue lives for all tested specimens. The experimental mean fatigue strength for all tested as-welded specimens is 108 MPa and the predicted value is 106 MPa. For the shot peened specimens the experimental mean fatigue strength is 119 MPa and the predicted 116 MPa. The predictions are in a good agreement with the experiments. The predicted fatigue strengths for the manual MCAW, Robotic MCAW and Manual FCAW are 103, 114 and 90 MPa, respectively. The experimental mean fatigue strengths are 98, 110 and 106 MPa, respectively. The predictions are within 5-15 % accuracy.

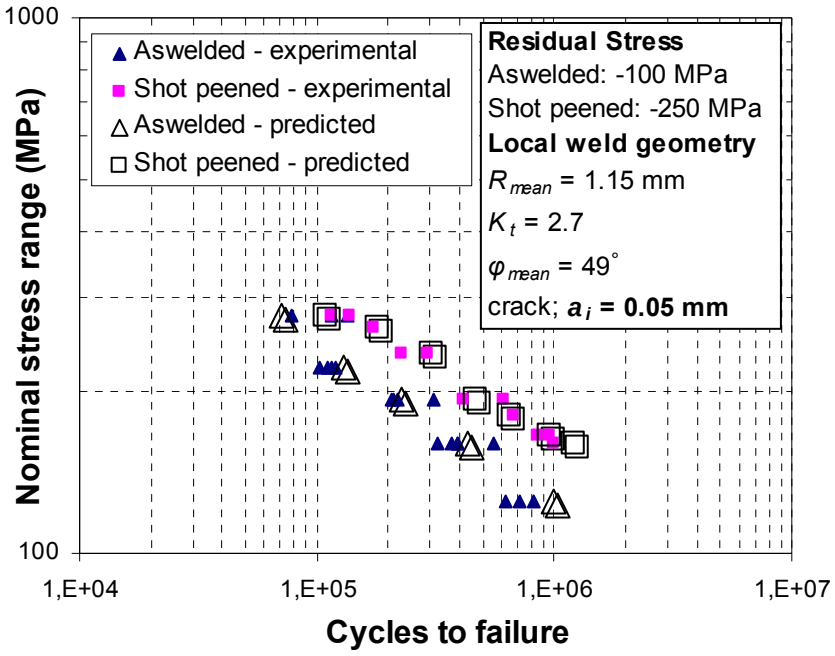


***Figure 11.*** *Predicted and experimentally obtained fatigue lives.*

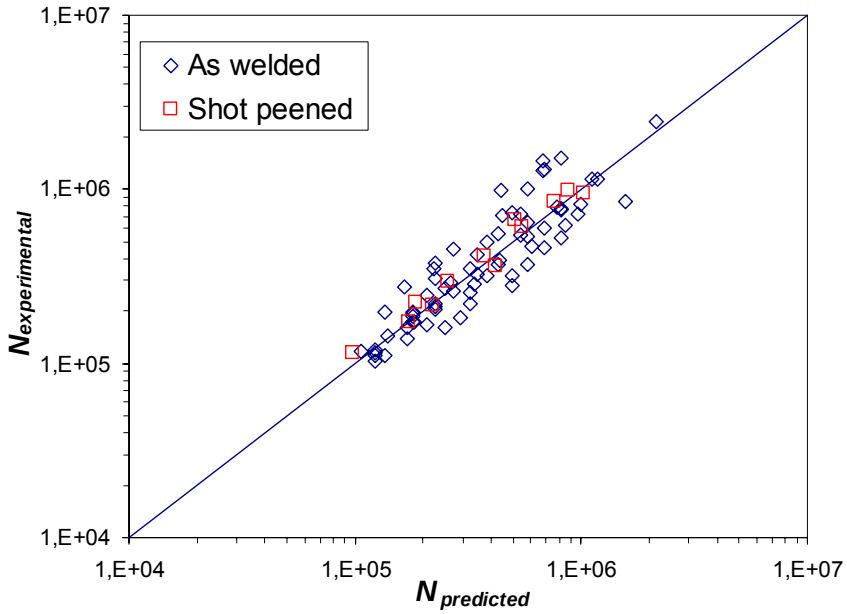


***Figure 12.*** *Comparison between experimental and predicted fatigue lives for: a) Manual MCAW; b) Robotic MCAW and c) Manual FCAW.*

### *Residual Stress effect on fatigue life*

Figure 13 shows the effect of different magnitudes of residual stress on the fatigue life. It can be clearly seen that the effect of the residual stress, compressive or tensile, is negligible at low fatigue lives and becomes more significant at lives $>10^5$ cycles. When considering tensile residual stresses (0 to 100 MPa), no significant change in the predicted fatigue life is observed. For example, the decrease in fatigue life due to a change from zero to 50 or 100 MPa tensile residual stress is only approx. 9-17% at an applied stress range of 200 MPa. However, in contrast, changing from a compressive residual stress of 200 MPa to a tensile one reduces the fatigue life at 200 MPa by 20 - 34%.

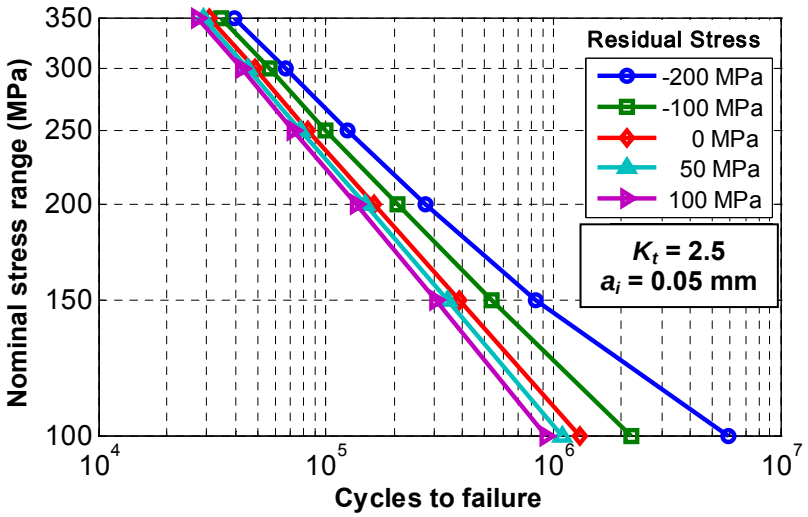


***Figure 13.*** *Influence of the magnitude of residual stress at weld toe for non-load carrying cruciform joints.*

***Crack growth from spatter - induced cold lap***

During the welding process a common phenomenon causing cold laps is spatter. A small drop of melted material falls ahead of the welding point and sticks to the surface of the plate. However, the drop is too small to be fully fused to the cold plate. Somewhat later, when the weld runs over, the small drop is partly melted and a small crack is left in the toe area of the weld. The form of the cold lap is thus a semi elliptical defect ($a/c$ = 1) rather than the usual assumption of a line cold lap ($a/c$ = 0). This later type, line cold lap ($a/c$ = 0), is often found when the welding speed is too high or if the plate is dirty or rusty. Similar behaviour can also be expected if there is a dirty spot at the material surface which may cause lack of fusion when welding, and hence a defect.
All the LEFM analyses described earlier in this paper were made using 2D FE models (assuming $a/c$ = 0). This is a conservative approach and since a spatter-induced cold lap is the most common type, it is important to investigate the difference between a line cold lap and a semi-elliptical spatter-induced cold lap. This requires a 3D LEFM analysis, where the cold lap is described as a semi-elliptic crack having $a/c$ = 1 at the start. Such an analysis was made using Franc3D [17] for a cruciform joint with thickness 12 mm, having a cold lap size of 0.2 mm at the sharp transition of the weld toe (radius = 0, angle 70˚) , see figure 14. The results is then compared with a 2D LEFM analysis of the same case, see figures 6 and 14 for comparison of the difference in crack shape and assessed life.
A theoretical view could argue that, for standard cases of surface cracks, the initial stress intensity factor $\Delta K_I$ for $a/c$ = 1 is only 63% of that for $a/c$ = 0. This would result in an increase in fatigue life by a factor of $0.63^{-3} \approx 4$. However, since the $a/c$ actually decreases during growth, the increase in life is smaller than this, as can be seen in figures 15 and 16.
The 3D LEFM analysis for the spatter induced cold lap shows that the start situation (at $a/c$ = 1) have a clear mixed mode loading condition which is quite different at the bottom (90˚) compared to the toe line (0˚ and 180˚), see figure 16.

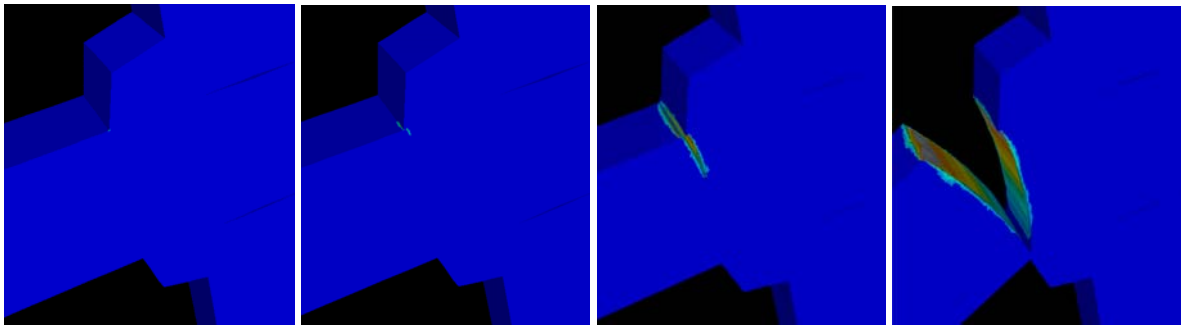

***Figure 14.*** *3D-model of a cold lap having a/c=1 at start. Pictures show the state from start (left with a/c = 1) to near failure (right with a/c ≈ 0.1). Due to symmetry only half a cold lap is modelled.*

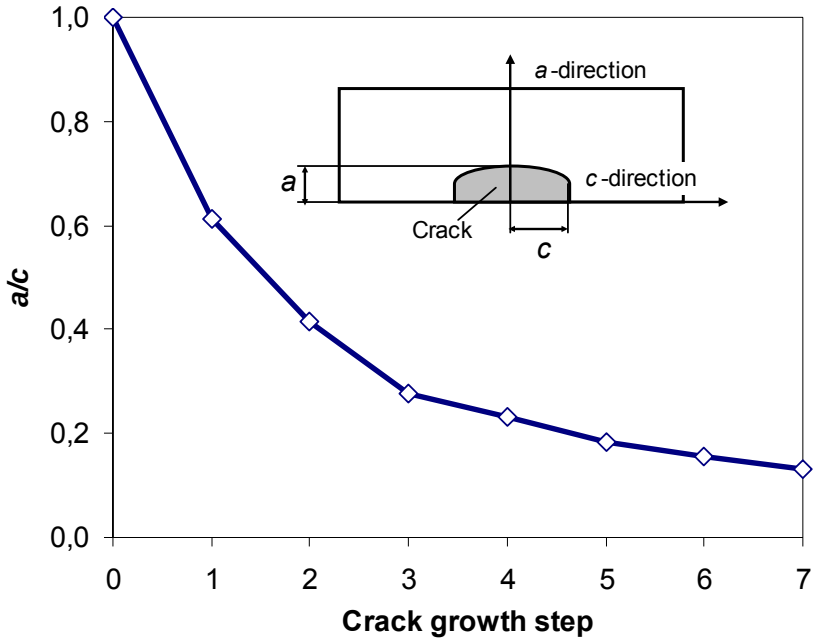


***Figure 15.*** *a/c relation during crack growth for the 3D LEFM analysis of a spatter- induced cold lap.*

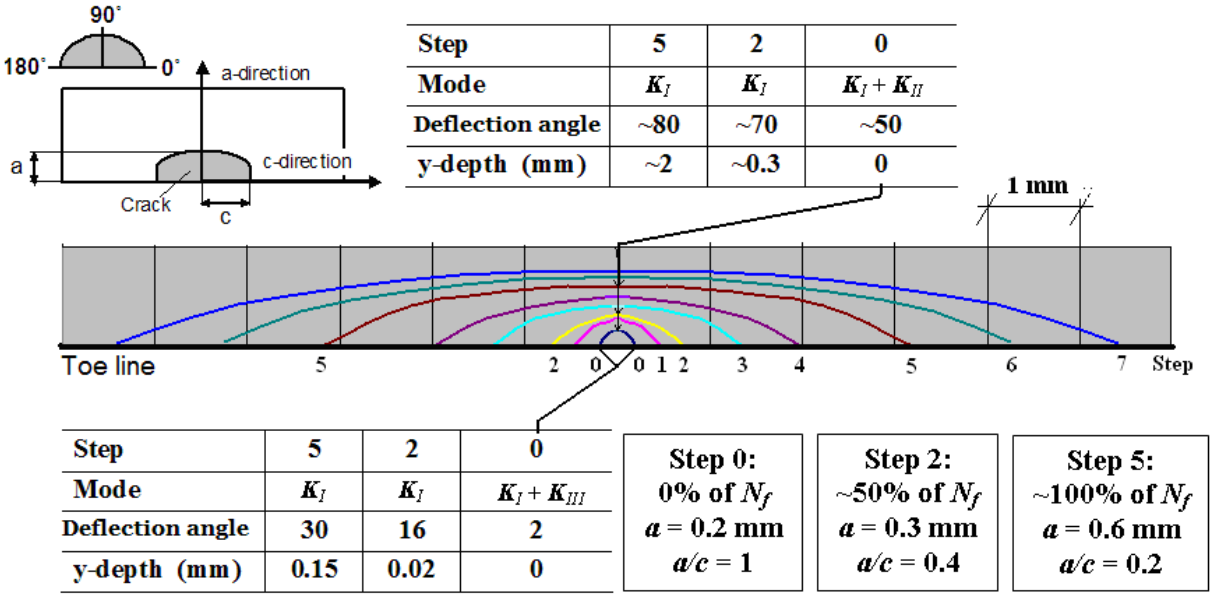


***Figure 16.*** *A top view of the crack shape of a 3D cold lap from start (step 0, a/c = 1) to approximately the end of life (step 7, a/c ≈ 0.1).*

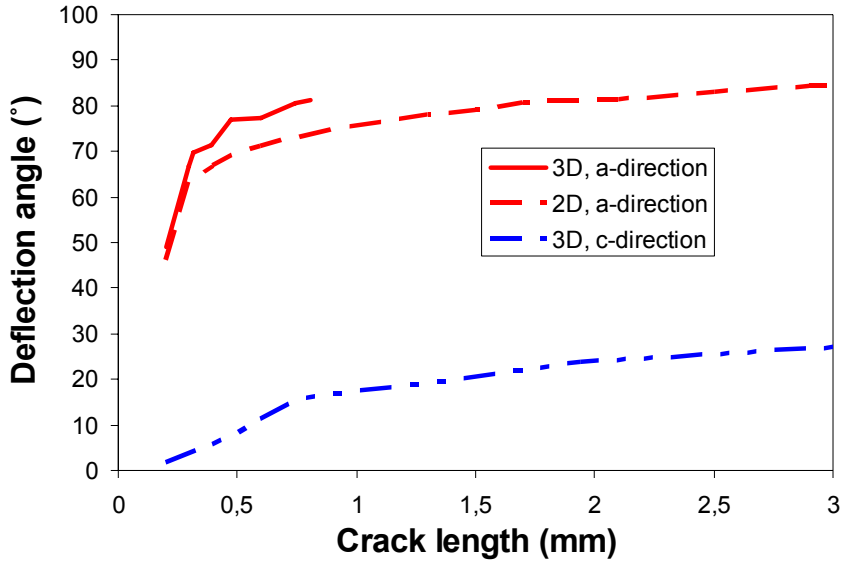


***Figure 17.*** *Comparison of deflection angles in 3D- and 2D LEFM –analysis of crack growth from spatter induced cold lap and line cold lap, respectively. Crack length is calculated using a+da and c+dc, respectively.*

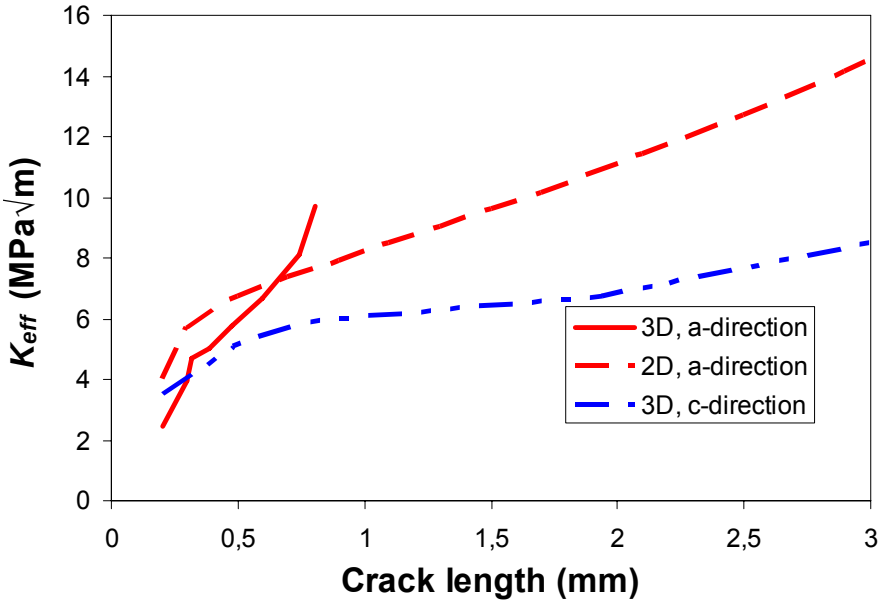


***Figure 18.*** *Effective stress intensity factor vs. crack growth for the 3D-2D LEFM analysis, respectively.*

At the start of crack growth, step 0 in Fig. 16, along the weld toe line (0˚ and 180˚, c-direction) the crack is under mixed mode, $\Delta K_I$ and $\Delta K_{III}$, i.e. the $\Delta K_I/\Delta K_{III}$ deflection angle is small ~2˚. The crack growth in the c-direction along the surface will dominate and crack growth into the depth is small. At the bottom (90˚, a-direction) the crack growth is under mixed mode $\Delta K_I$ and $\Delta K_{II}$ leading to a much greater deflection angle ~50˚. This is in excellent agreement with the previous 2D LEFM crack growth analysis for a line cold lap, where the deflection angle is identical at the crack growth start, see figure 17-18. Figure 18 also shows the small deflection angle in the c-direction, i.e. $\Delta K_I/\Delta K_{III}$ deflection angle. The crack grows quickly in the depth direction. After the first crack growth step the mixed mode quickly

diminishes and mode I crack propagation will dominate the subsequent crack growth steps both in the *a*-and *c*- direction. The a/c relation decreases rather slowly to approximately 0.1-0.2 at the last crack growth step, see figure 15.
For the 3D case the fatigue life is calculated automatically after curve fitting $\Delta K_{eff}$ and crack length. The crack propagation direction is calculated with the mixed mode interaction theory according to the maximum hoop stress criterion.
The fatigue life calculations for the two cases show that the semi elliptical 3D case (spatter-induced cold lap) has a life of 2.7 million cycles, where the line cold lap in the same situation has a life of 1 million cycles, see figure 19. This means that the theoretical factor 4 is not reached; instead a factor 2.7 is appropriate.

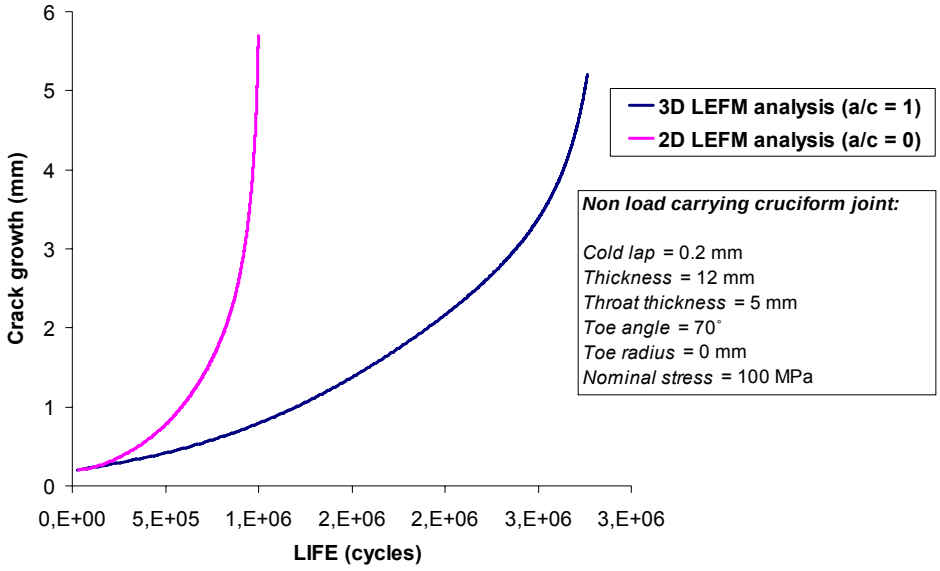


***Figure 19.*** *Comparison of fatigue life for a line cold lap (a/c=0) and a spatter- induced cold lap (a/c=1).*

## Discussion

In this investigation fatigue tests have been performed on non load carrying cruciform joints welded with different welding processes. The fatigue tested specimens were as welded and shot peened. The weld quality and the local weld geometry variation were also studied. The theoretical fatigue results were predicted using linear elastic fracture mechanics and then compared with the test results.
The shot peened batches show higher fatigue strength due to the compressive residual stress induced. However, defects survived after this post weld improvement process and were of the same size as the as-welded detected defects. This is observed in an earlier non-published work within a Nordic project. The difference in the local weld toe geometry was significantly smaller after the shot peening due to the removal of a thin line of slag. The *Robotic MCAW* as-welded batch showed a slightly higher characteristic fatigue strength (fatigue strength at 5 % failure probability, *FAT*), 71 MPa, and lower stress concentration compared with the *Manual MCAW* batch, 70 MPa, although the *Robotic MCAW* batch exhibited more scatter in fatigue lives.
The specimens in the *Manual FCAW* batch were brushed before local weld geometry measurement and fatigue testing. This contributed to the small scatter in the local weld

geometry measurements compared to specimens welded with *MCAW*. After the measurement of the local weld geometry, undercuts were detected in the specimens from the *Manual FCAW* batch. The fatigue strength was higher for this batch, 80 MPa, and was in agreement with the IIW fatigue strength class recommendation for non-load carrying cruciform joints, *FAT* 80.

The microscopic investigation showed cold lap defects along the weld toe of various sizes and shapes. It was often difficult to estimate the sizes of single cold laps since they were scattered along the weld bead and accompanied by spatter. These cold lap defects contributed to the scatter in the fatigue testing results.

The fatigue life of welded joints in the real world involves propagation under plane strain conditions due to the larger thicknesses in welded structures. However, plane stress is a more conservative assumption than plane strain, i.e. worst case (deterministic). The location of the initial crack could have a significant influence on the predicted fatigue life. In this study the initial location of the crack was assumed to coincide with the maximum stress concentration. This is somewhat conservative and warrants further statistical analysis, since the particular defect size analyzed and maximum stress concentration will not necessarily coincide.

Another conservative assumption used is the 2D case. This means implicitly that $a/c = 0$ and is valid for a line cold lap. However, most cold laps occur when spatter is involved and would therefore be expected to have a semi-elliptical form; in the present analysis this was assumed to correspond to $a/c = 1$. This results in a longer life, since simple formulae for stress intensity factors give lower values for this case. The 3D LEFM analysis showed that the semi- elliptical cold lap with $a/c = 1$ will propagate with mixed mode which varies along the crack front. The 3D LEFM analysis corresponds very well to the 2D LEFM analysis at the bottom (depth) of the crack at the start of crack propagation. The direction of the crack growth suddenly changes to mode I and continues to propagate in mode I with low $\Delta K_{II}$ and $\Delta K_{III}$. The calculated life for a semi elliptical crack was in one case nearly 3 times longer than that for a line cold lap. This was also confirmed by a 2D LEFM analysis of a semi-elliptical surface flaw which gave 2.7 times longer fatigue life than a line cold lap. It could be argued that spatter-induced cold laps are not as dangerous as cold laps induced by excessive welding speed or a poor plate surface, where line cold laps could be expected to form.

The microscope analysis of the fractured specimens showed that fatigue cracks propagated from spatter-induced cold lap defects as mode I surface cracks right from the start. This is in good agreement with the fracture mechanics simulations of crack growth from cold lap defects, where the kink angle immediately becomes large and very soon reaches a value around 90 degrees. This means that most of the fatigue life is consumed in the first steps of the crack growth, and the cold lap defect continues to grow as a surface crack. Hence, the cold lap defect could be represented as an equivalent initial surface crack.

The fatigue strength is increased for toe radii larger than 1 mm and for cold lap defects smaller than 0.5 mm. This shows the importance of minimizing the cold lap defect sizes and increasing the toe radius in order to increase the fatigue strength of a weld, although the cold lap defect size is predominant.

## Conclusions

1. No large defects were present in the analyzed batches. The common defect found was cold laps in connection with spatter.

2. Good fatigue strength and relatively small scatter was observed for specimens welded with manual FCAW.

3. The shot peening removed slag and some larger spatter along the weld toe and resulted in smaller measured toe radius and toe angle. As a consequence, the stress concentration factor was under-estimated if it was based on measurements made before shot peening.

4. Consequently, before measurement of the local weld geometry, the specimens should be brushed and cleaned from loose slag and spatter that could complicate the measurement of the real toe radius and toe angle.

5. The effective notch stress design curves (5% probability of failure) for the all batches were all below the IIW recommendation; *FAT* 225 MPa.

6. The weld toe radius should be larger than 1 mm (with an even transition) and the cold lap defect size smaller than 0.5 mm in order to assure a *FAT* 80 weld.

7. 3D analysis indicates that spatter-induced cold laps having a semi-circular form could be expected to have 2-3 times longer life than line cold laps.

8. By incorporating the residual stresses the LEFM fatigue life assessment showed good correlation with experiments when assuming a 0.05 mm initial surface crack representing a cold lap defect at the weld toe.

## Acknowledgements

Mr. Ruben Fernandez Ricondo at the Royal Institute of Technology is greatly acknowledged for carrying out laboratory work. Dr Abdul-wahab Fethi at Volvo Metal Lab is also acknowledged for assistance in the fracture mechanical analysis. Prof. S.J. Maddox at TWI is acknowledged for reading trough the manuscript.

## References

1. Barsoum Z., Fatigue and quality analysis of cruciform joints welded with different methods, IIW doc. IIW-XIII-2136-06 (2006).

2. Barsoum Z. and Samuelsson J., Fatigue assessment of cruciform joints welded with different methods, Steel Research International 77, No. 12, pp. 882-888, (2006).

3. Martinson J., Fatigue assessment of complex welded structures, Doctoral Thesis, Dept. of Aeronautical and Vehicle Engineering, KTH, Sweden 2005, ISBN 91-2783-968-6.

4. Samuelsson J., Cold laps and weld quality acceptance limits, Design and Analysis of Welded High Strength Steel Structures, pp. 151-163, Stockholm, EMAS, 2002.

5. Samuelsson J., Fatigue design of vehicle components methodology and applications, Dept. of Aeronautical Structures and Materials, Report no.88-23, Doctoral Thesis, The Royal Institute of Technology, Stockholm, 1988.

6. Barsoum Z., Weld quality assessment of test specimens, report 2003-9, Master thesis, Department of Aeronautical and Vehicle Engineering, Royal Institute of Technology, 2003, Stockholm.

7. Barsoum Z., Residual Stress Analysis and Fatigue of Welded Structures, Licentiate Thesis, Dept. of Aeronautical and Vehicle Engineering, KTH, Sweden 2006, ISBN 91-7178-264-8.

8. Hobbacher A., Fatigue design of welded joints and components, IIW doc. XX-1539-96.

9. Lopez Martinez L., Korsgren P., Characterization of initial defect distribution and weld geometry in welded fatigue test specimens, Fatigue under Spectrum Loading and Corrosive Environment, pp. 3-21, Warley, UK, EMAS, 1993.

10. Signes, E.G et al, Factors affecting the fatigue strength of welded high strenght steels, Brit. Welding Journal., 14(3), pp108-116, 1967.

11. Lundin M., Lopez Martinez L., Hedegård J., Weman K., High productive welding - fatigue properties of weldments, Welded High Strength Steel Structures, pp. 33-47, Stockholm oktober 1997, Blom A.F., EMAS.

12. Lopez Martinez L., Fatigue behaviour of welded high-strength steels, report 1997-30, Doctoral dissertation, Department of Aeronautical and Vehicle Engineering, Royal Institute of Technology, 1997, Stockholm.

13. FRANC2D. Version 3.2 http://www.cfg.cornell.edu/

14. AFGROW. Version 4.0005. http://fibec.flight.wpafb.af.mil/fibec/afgrow.html

15. Nykänen T., Marquis G., Björk T., Fatigue analysis of non-load-carrying fillet welded cruciform joints, Engineering Fracture Mechanics, vol 74, pp. 399-415, 2007.

16. Forman, R.G., and Mettu, S.R., Behavior of surface and corner cracks subjected to tensile and bending loads in Ti-6Al-4V alloy, Fracture Mechanics 22nd Symposium, Vol. 1, ASTM STP 1131, H.A. Ernst, A. Saxena and D.L. McDowell,eds., American Society for Testing and Materials, Philadelphia, 1992.

17. FRANC3D. Version 3.1 http://www.cfg.cornell.edu/